IEEE Access
Multidisciplinary | Rapid Review | Open Access Journal

Received February 29, 2020, accepted March 19, 2020, date of publication March 23, 2020, date of current version April 7, 2020.

Digital Object Identifier 10.1109/ACCESS.2020.2982845

A Calibration Method Based on Transfer Function Extraction for Cartesian Vector Modulator

CHAO WANG[1,2], XIANG-RUI CHENG[1], YIN-XIN SUN[1], PENG-SONG DUAN[1,2], AND YANG-JIE CAO[1,2]

[1]School of Software, Zhengzhou University, Zhengzhou 450000, China
[2]Hanwei Internet of Things Research Institute, Zhengzhou University, Zhengzhou 450000, China

Corresponding author: Yang-Jie Cao (caoyj@zzu.edu.cn)

This work was supported by the Nature Science Foundation of China under Grant 61972092.

ABSTRACT In this paper, a calibration approach based on transfer function extraction for the Cartesian vector modulator (VM) is presented. Three kinds of VM models—the ideal VM model, the frequency-dependent VM model and the modified frequency-dependent VM model, are introduced in the proposed calibration approach. The calibration approach starts with an initialization of the transfer function of the modified frequency-dependent VM model. Then, the parameters of the transfer function are modified and extracted from the data of the measured transmission state (transmission amplitude and phase) of the actual VM by iteration, until the transmission state predicted by the extracted transfer function agrees well with the measured transmission state. Subsequently, the extracted transfer function of the modified frequency-dependent VM model is capable of describing the transmission characteristics of the actual VM, and the calibrated baseband control voltages for the desired transmission amplitude and phase of the actual VM are able to be obtained by using the extracted transfer function. An actual VM is used as an example to verify this method. By adopting the proposed method, the maximum amplitude and phase errors at different complex gain setpoints are reduced to 0.05 dB and 0.3° respectively after only two iteration steps. Since the actual VM is able to be accurately calibrated in only a few iteration steps, the results reveal that high accuracy and efficiency can be obtained in this calibration technique, which is well suited for applications involving high-accuracy calibration, real-time calibration and multichannel VM system calibration.

INDEX TERMS Calibration, gain control, phase control, transfer function, vector modulator (VM).

I. INTRODUCTION

The vector modulator (VM) plays an important role in a variety of applications, in which the amplitude and phase control of signals are required, particularly in beamforming and phased array systems [1]–[3], modern communication systems [4]–[6], fifth-generation (5G) mobile technology [7]–[10], and feed-forward linearization techniques [11]–[13].

Traditionally, the VM can be divided into four main categories [6], [14], [15]: polar-based [16], phase oversampling [14], constant-Gm [15], and Cartesian-combining types [6]. Comparatively, the Cartesian-combining VM is more widely used [3], [17]–[21] due to the ease of implementation and manipulation, low cost and widespread commercial availability.

The associate editor coordinating the review of this manuscript and approving it for publication was Wei Liu.

The control accuracy of the transmission amplitude and phase of the VM is of essential importance in many application scenarios. In phased array antennas and beamforming applications, the precision of the radiation pattern relies on the accuracy of the amplitude and phase of the RF signals [21], [22]. Meanwhile, the beamforming performance and the electrical steering performance of a phased array system depend mostly on the resolution of the controlled phase shift [23]. For communication systems, the control accuracy of the transmission phase and amplitude of the VM are crucial to provide an accurate constellation [24]. However, it is difficult to obtain the desired transmission amplitude and phase with high resolution and accuracy. For an actual Cartesian VM, the control accuracy of the transmission phase and amplitude are degraded by the asymmetry in the in-phase (I) and quadrature (Q) signal paths, the nonideal behavior of the quadrature hybrid and the amplitude modulators, and other imperfections [17]. Therefore, a careful calibration procedure should be adopted. In [23], [25]–[27], the calibration

was implemented by sweeping the control voltages of the VM while measuring its corresponding transmission state, and then search through the measured transmission states to find which are closest to the desired transmission states. By developing an appropriate data selection technique to reduce the testing data points on the constellation, a relatively efficient calibration approach is realized [28]. The relationship between the calibrated control signals and the desired phase shift was developed in [29], and the coefficients of the developed transfer functions were obtained by performing power measurements. A model-based calibration method mainly concerned with the amplitude and phase imbalance of the quadrature generator network of the VM was presented in [30], and the unknown values of the model parameters were experimentally determined. A feed-forward calibration method based on the predistortion concept was introduced in [17], and a lookup table was employed to store the correction parameters of the transmission amplitude and phase, which were obtained through measurements.

The calibration works presented above are grouped into two types: the sweep control signal method [23], [25], [26], [28] and the model-based method [17], [29], [30]. For the first type, the I and Q control voltages of the VM are swept over a two-dimensional array [26] and the transmission states of the VM are measured at each point on the two-dimensional control voltage plane, then the calibration is finished by choosing the best matched transmission state with respect to the desired transmission state. It is relatively simple to obtain the required control signals for the desired transmission states by using this method. It should be noted that, as the I and Q control voltages have to sweep over a two-dimensional array, the step size and the sweep area of the control voltages determine the number of the testing points on the control voltage plane. When high-resolution and high-accuracy along with large control range are desired for the transmission states, a small step size and a large sweep area would be required for the I and Q control voltages. However, this would result in a large number of testing points on the control voltage plane, leading to a time-consuming and inefficient measurement. Therefore, when adopting this technique, a trade-off between the calibration accuracy and the time consumption should be considered. Furthermore, this method is not very suited for the calibration of the multichannel VM system and the real-time calibration scenarios. The second approach typically introduces a model and the corresponding transfer functions, which relate the control signals and the transmission state of the VM. By performing a set of measurements, the parameters of the transfer functions are extracted, and then the required control signals for the desired transmission state are able to be calculated by using the extracted transfer functions. In [29], [30], the procedure for the parameters extraction is to sweep the parameters of the proposed transfer function until the predicted characteristics by the extracted transfer function agree well with the measured characteristics of the actual VM. The VM model and the calibration approach proposed in [17] are capable of calibrating the transmission state of the VM with high accuracy and efficiency, but the inherent frequency-dependent insertion phase and loss of the actual VM are not included in the proposed VM model.

In this paper, a calibration method based on transfer function extraction for the Cartesian VM is presented. In order to obtain the transfer functions of the actual VM, three VM models, the ideal VM model, the frequency-dependent VM model and the modified frequency-dependent VM model, and their corresponding transfer functions are developed. The modified frequency-dependent VM model is a behavioral model of the actual VM, which is not restricted to the specific nonideal behavior of the actual VM and takes into account the frequency-dependent insertion phase and loss of the actual VM. Through a few iterations, the transfer functions of the modified frequency-dependent VM model are able to be accurately extracted from the measured transmission amplitude and phase of the actual VM. Subsequently, the calibrated baseband control voltages for the desired transmission state of the actual VM are able to be obtained. The experimental results show that the errors of the calibrated transmission amplitude and phase are less than 0.05 dB and 0.3°, respectively, after only two iteration steps. Due to the high accuracy and efficiency of the proposed calibration method, it is well suited for the multichannel VM system and the real-time calibration scenarios, such as the phased array systems and the low-level RF control system for accelerators [17], [19].

The rest of this paper is organized as follows. In Section II, three kinds of VM models and the principle of the transfer function extraction for the Cartesian VM are described. In Section III, a practical example is given to validate the proposed calibration approach. A discussion of the measurement results is presented in Section IV. Finally, the conclusions are drawn in Section V.

II. THE PRINCIPLE OF TRANSFER FUNCTION EXTRACTION FOR THE CARTESIAN VM

The objective of the transfer function extraction for the Cartesian VM is to find a series of parameters of a predefined model, whose response agrees well with a given set of measurement data. To investigate the principle of the transfer function extraction in this paper, it is necessary to discuss the Cartesian VM first.

A. CARTESIAN VM AND THE IDEAL VM MODEL

The functional blocks of a Cartesian VM are illustrated in Fig. 1.

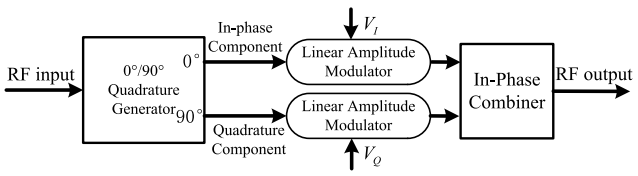

FIGURE 1. Block diagram of the Cartesian VM.

First, the RF input signal is applied to the quadrature generator network, which splits the signal into I and Q components. Then, the I and Q signals are weighted by two linear amplitude modulators individually, and the weighted values of the I and Q signals are controlled by Cartesian baseband inputs V_{I} and V_{Q}, respectively. Eventually, the two amplitude-modulated I and Q signals are combined by an in-phase combiner to form the RF output signal, whose amplitude and phase are able to be adjusted simultaneously and continuously by controlling V_{I} and V_{Q}. By assuming that the circuit components of the VM in Fig. 1 have ideal characteristics and are frequency-independent, this VM can be regarded as the ideal VM model. Then, the relationship between the transmission coefficient (S21) and the baseband control voltages (V_{I}, V_{Q}) of the ideal VM model is given by [20]:

$$|S21| \propto \sqrt{V_I^2 + V_Q^2} \tag{1a}$$

$$\angle S21 = \arctan \frac{V_Q}{V_I} \tag{1b}$$

According to equation (1), the contour plots of the transmission amplitude (|S21|) and phase (∠S21) of the ideal VM model are able to be simulated, and are illustrated in Fig. 2.

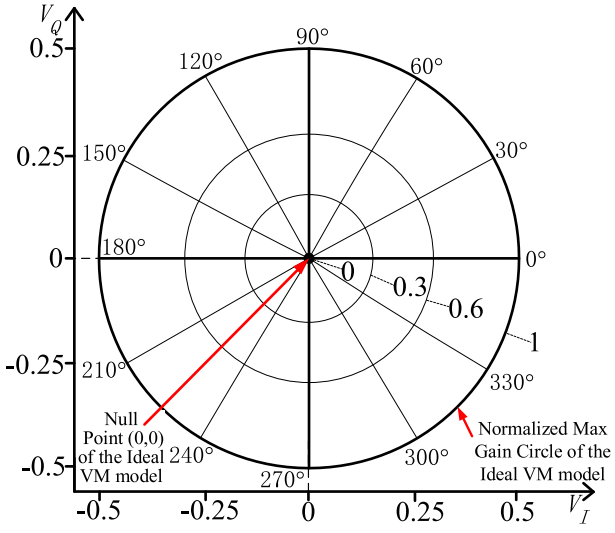

FIGURE 2. Simulated contour plots of the transmission amplitude and phase of the ideal VM model.

From this figure, the null point of the transmission amplitude of the ideal VM model is located at the origin of the coordinate system. The contour plots of the transmission amplitude are represented by a series of concentric circles around the null point, and the contour plots of the transmission phase exhibit a set of straight lines starting from the null point. It is worth mentioning that there is only one intersection point between a certain transmission amplitude contour line and a certain transmission phase contour line. It indicates that the required baseband control voltages for the desired transmission coefficient are unique. Therefore, the problem of obtaining the required baseband control voltages for the desired transmission state can be converted to the problem of: finding the position (coordinate values) of the intersection point of the desired transmission amplitude contour line and the desired transmission phase contour line.

In practice, since the actual VM exhibits frequency-dependent properties and nonideal behavior, equation (1) could hardly describe the transfer characteristics of the actual VM. Therefore, a more practical transfer function should be developed.

B. THE FD-VM MODEL AND THE MODIFIED FD-VM MODEL

Before developing a more practical VM model and the corresponding transfer function, it is beneficial to investigate the structure of the actual VM. Fig. 3(a) and Fig. 3(b) show an actual multichannel VM module and a single VM channel, respectively. From Fig. 3(b), it shows that the actual VM consists of the VM core circuit and the input/output transmission lines. The VM core circuit is composed of the VM chip and the associated distributed components. Usually, the performance of the VM chip and the distributed components are frequency-dependent. Meanwhile, the insertion phase and loss of the input/output transmission lines are also frequency-dependent. Therefore, the frequency-dependent characteristics presented in the VM core circuit and the input/output transmission lines would contribute to the overall frequency-dependent property of the actual VM, and these frequency-dependent insertion loss and phase properties of the actual devices should be considered in a more practical VM model.

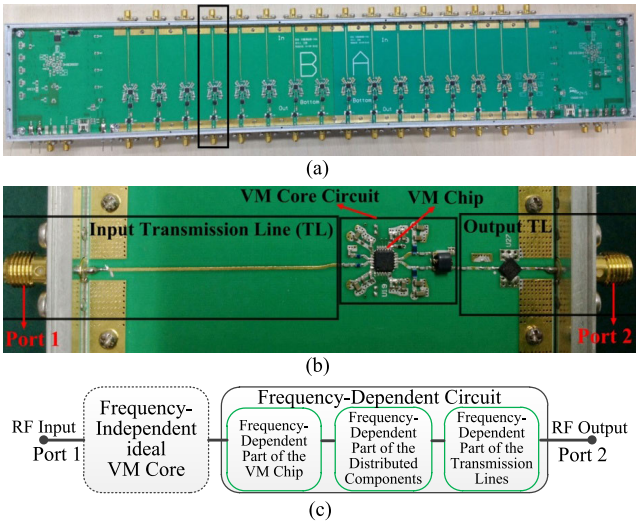

FIGURE 3. (a) Photograph of an actual multichannel VM module. (b) A single VM channel. (c) Block diagram of the FD-VM model.

Based on the descriptions presented above, a relatively practical VM model named as the frequency-dependent VM (FD-VM) model is introduced, which is shown in Fig. 3(c). The FD-VM model is composed of the frequency-independent ideal VM core and the frequency-dependent circuit. The vector modulation function of the

FD-VM model is realized by the frequency-independent ideal VM core, whose transfer function is identical with that of the ideal VM model. The frequency-dependent circuit of the FD-VM model contains all of the frequency-dependent aspects in the actual devices. Therefore, the transfer function of the FD-VM model, which is shown in equation (2), is regarded as a modification of the transfer function of the ideal VM model by adding frequency-dependent terms.

$$Gain\left(V_{BBI}, V_{BBQ}, f\right) = 20\log_{10}\sqrt{\left(\frac{V_{BBI}}{V_O}\right)^2 + \left(\frac{V_{BBQ}}{V_O}\right)^2} + Gain_{const}\left(f\right)(dB) \tag{2a}$$

$$Phase\left(V_{BBI}, V_{BBQ}, f\right) = \arctan\frac{V_{BBQ}}{V_{BBI}} + Phase_{const}\left(f\right)(Deg) \tag{2b}$$

In equation (2), *Gain* (V_{BBI}, V_{BBQ}, f) and *Phase* (V_{BBI}, V_{BBQ}, f) represent the transmission amplitude and phase of the FD-VM model, respectively. $Gain_{\mathrm{const}}(f)$ is the insertion loss of the total frequency-dependent part of the actual VM, which corresponds to the insertion loss of the frequency-dependent circuit of the FD-VM model. $Phase_{\mathrm{const}}(f)$ is the systematic insertion phase of the actual VM, which corresponds to the insertion phase of the frequency-dependent circuit of the FD-VM model. V_{BBI} and V_{BBQ} are the I and Q channel baseband control voltages, respectively. V_{o} is the baseband scaling constant, which is used to set the maximum transmission amplitude of the actual VM. V_{o} is decided and provided by the manufacturer of the VM. Similar to the analysis of the ideal VM model, the contour lines of the transmission amplitude of the FD-VM model are represented by a series of circles centered at (0, 0), and the contour lines of the transmission phase exhibit a set of straight lines starting from (0, 0).

Through a large number of measurements, it is found that the calibration accuracies of the transmission amplitude and phase of the FD-VM model are approximately 5 dB and 10°, respectively. It reveals that the FD-VM model is only able to be used as a relatively coarse model for VM calibration, it is not sufficient for high-accuracy applications, in which the errors of the transmission amplitude and phase may be less than 0.1 dB and 1°, respectively. Therefore, the FD-VM model should be modified in order to obtain high calibration accuracy.

In the FD-VM model, the amplitude null point is located at (0, 0) in the V_{BBI}-V_{BBQ} plane. However, in real applications, the null point of the actual VM would be deviated from (0, 0). Considering this nonideal characteristic, the transfer function of the FD-VM model is modified as:

$$Gain\left(V_{BBI}, n_I, V_{BBQ}, n_Q, f\right) = \underbrace{20\log_{10}\sqrt{\left(\frac{V_{BBI}-n_I}{V_O}\right)^2+\left(\frac{V_{BBQ}-n_Q}{V_O}\right)^2}}_{a} + Gain_{const}\left(f\right)(dB) \tag{3a}$$

$$Phase\left(V_{BBI}, n_I, V_{BBQ}, n_Q, f\right) = \underbrace{\arctan\frac{V_{BBQ}-n_Q}{V_{BBI}-n_I}}_{b} + Phase_{const}\left(f\right)(Deg) \tag{3b}$$

Equation (3) is the transfer function of the modified FD-VM model. *Gain* (V_{BBI}, n_{I}, V_{BBQ}, n_{Q}, f) and *Phase* (V_{BBI}, n_{I}, V_{BBQ}, n_{Q}, f) represent the transmission amplitude and phase of the modified FD-VM model, respectively. The terms a and b are the modified transfer function of the transmission amplitude and phase of the ideal VM model, respectively. n_{I} and n_{Q} are the coordinate values of the transmission amplitude null point of the modified FD-VM model, on the $V_{\mathrm{I-axis}}$ and $V_{\mathrm{Q-axis}}$, respectively. Similar to the analysis of the ideal VM model, the contours of the transmission amplitude of the modified FD-VM model are represented by a series of circles centered at (n_{I}, n_{Q}), and the contours of the transmission phase exhibit a set of straight lines starting from (n_{I}, n_{Q}). Equation (2) is a special case of equation (3) when both n_{I} and n_{Q} are equal to zero, and the contours of the transmission amplitude and phase of equation (3) are the translation of those of equation (2) by vector (n_{I}, n_{Q}).

C. TRANSFER FUNCTION EXTRACTION

In practice, the transfer function of the actual VM should be obtained, in order to get the baseband control voltages for the desired transmission amplitude and phase. To illustrate the transfer function of an actual VM at a certain frequency point, its contour plots of the transmission amplitude and phase are assumed to be ellipses and straight lines respectively, which are sketched in Fig. 4.

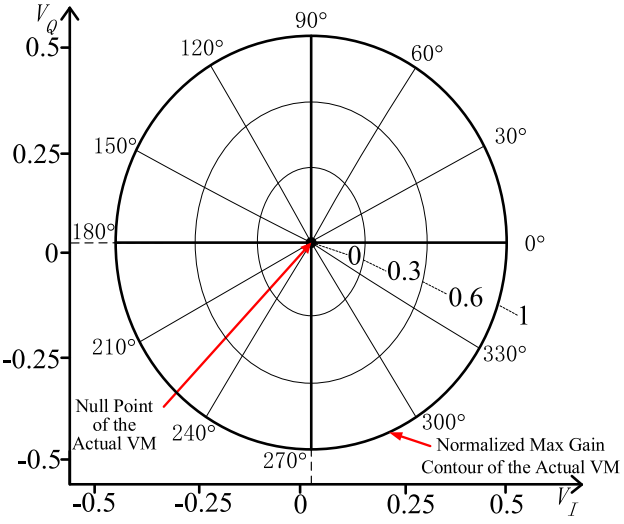

FIGURE 4. Sketch illustrating the contour plots of the transmission amplitude and phase of the actual VM at frequency f.

In this figure, due to the nonideal behavior of the actual VM, the amplitude null point is deviate from (0, 0), and the amplitude contours are represented by ellipses, but not circles. If the curve functions of the transmission amplitude and

phase contours are achieved, the required baseband control voltages for the desired transmission amplitude and phase are able to be calculated directly. Unfortunately, these functions are usually unknown and cannot be determined easily and accurately. Therefore, it is necessary to investigate a method to obtain the transfer function of the actual VM.

The main idea of the proposed transfer function extraction and the VM calibration method are that, by shifting the contours of the transmission amplitude and phase of the FD-VM model in the V_I-V_Q plane, these contours are able to be coincided with the contours of the transmission amplitude and phase of the actual VM at the desired transmission state point. Then, the shifted contours of the transmission amplitude and phase of the FD-VM model, which correspond to the contours of the transmission amplitude and phase of the modified FD-VM model, are applied to predict and calibrate the transmission characteristics of the actual VM at the desired transmission state point.

To describe the procedure of the proposed calibration method in a convenient way, the contours of certain transmission amplitude and phase of the actual VM and the FD-VM model are sketched in Fig. 5. In this figure, the solid ellipse and line represent the A (dB) amplitude and the θ (degrees) phase contours of the actual VM respectively, while the dotted circle and straight line represent that of the FD-VM model. The contours of A (dB) and θ (degrees) of the actual VM intersect at point A. It indicates that, if the desired amplitude and phase for the actual VM are A (dB) and θ (degrees) respectively, the coordinate values of point A, which correspond to the baseband control voltages for the desired transmission state, should be obtained. Therefore, the problem of achieving the desired transmission state is converted to obtain the coordinate values of point A. It is notable that, the A (dB) and θ (degrees) contours of the FD-VM model intersect at point B, and point A and point B will coincide, if ideal performance is achieved for the actual VM.

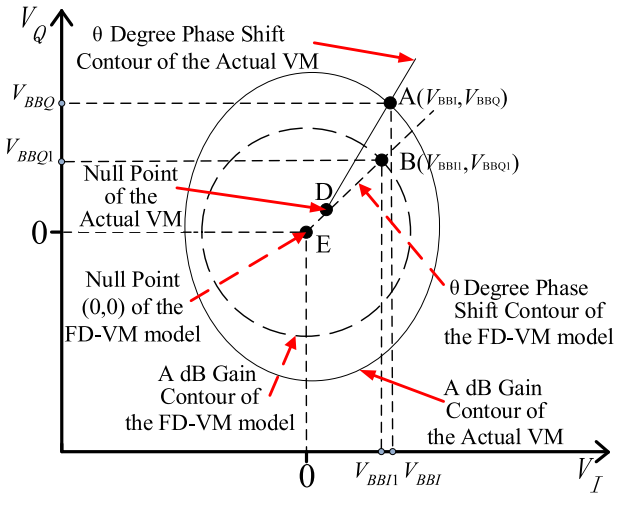

FIGURE 5. Sketch illustrating the transmission amplitude, A, and phase shift, θ, contours of the actual VM and the FD-VM model at frequency f.

However, due to the nonideal behavior of the actual VM, there is some deviation between point A and point B. As mentioned in Section II. B, the FD-VM model can be regarded as a coarse model to describe the transfer function of the actual VM, therefore, the coordinate values (V_{BBI1}, V_{BBQ1}) of point B are regarded as the initial baseband control voltages for the desired transmission state of the actual VM. By substituting the desired transmission state into equation (2), V_{BBI1} and V_{BBQ1} are obtained, which are regarded as the preliminary coordinate values of point A. The validity of the preliminary values is able to be verified by applying V_{BBI1} and V_{BBQ1} to the actual VM and measure the corresponding transmission coefficient. The measured transmission amplitude and phase are assumed to be A_{m1} and θ_{m1} respectively, if A_{m1} and θ_{m1} are within the tolerance of the desired transmission state, then V_{BBI1} and V_{BBQ1} are the required baseband control voltages. This situation occurs when low accuracy is required for the transmission state, but it is no longer the case in high-accuracy applications. The FD-VM model is only applicable for a coarse calibration, and a further calibration step should be adopted if more accurate calibration results are required.

To obtain the control voltages for point A more accurately, intuitively, shift the contours of the FD-VM model and point B will shift to a new position point B', which is closer to point A. Then, this new point is supposed to predict point A. As illustrated in Fig. 6(a), the center of the amplitude contour of the FD-VM model is shifted from the origin point E (0, 0) in Fig. 5 to point E' (n_{I1}, n_{Q1}) in Fig. 6(a), and point B is shifted to the new position point B' by vector (n_{I1}, n_{Q1}). n_{I1} and n_{Q1} represent the shift values of the contours of the FD-VM model on the V_{I-axis} and V_{Q-axis}, respectively. Meanwhile, n_{I1} and n_{Q1} are also the coordinate values of the transmission amplitude null point of the modified FD-VM model. In the procedure of the transfer function extraction, the contours of the FD-VM model are shifted by vector (n_{I1}, n_{Q1}), therefore, (n_{I1}, n_{Q1}) is also named as the shift vector pair. In order to obtain the coordinate values of point B', the values of n_{I1} and n_{Q1} must be obtained first. As the measured transmission state of the actual VM is known when the baseband control voltages are V_{BBI1} and V_{BBQ1}, then the mapping between the measured transmission state (A_{m1} and θ_{m1}) and the corresponding baseband control voltages (V_{BBI1}, V_{BBQ1}) for the actual VM is able to be obtained. For the FD-VM model, V_{BBI1} and V_{BBQ1} are correspond to the transmission state of A and θ rather than A_{m1} and θ_{m1}. Assuming that the relationship between (V_{BBI1}, V_{BBQ1}) and (A_{m1} and θ_{m1}) for the actual VM, corresponds to the intersection point of the A_{m1} amplitude contour and the θ_{m1} phase contour of the modified FD-VM model, which is illustrated as point G in Fig. 6(b). Subsequently, the transfer function of the actual VM for this transmission state (A_{m1} and θ_{m1}) can be formulated in equation (3).

Equation (3) denotes the functional relationships between three parameters: the baseband control voltage pair (V_{BBI}, V_{BBQ}), the shift vector pair (n_I, n_Q) and the

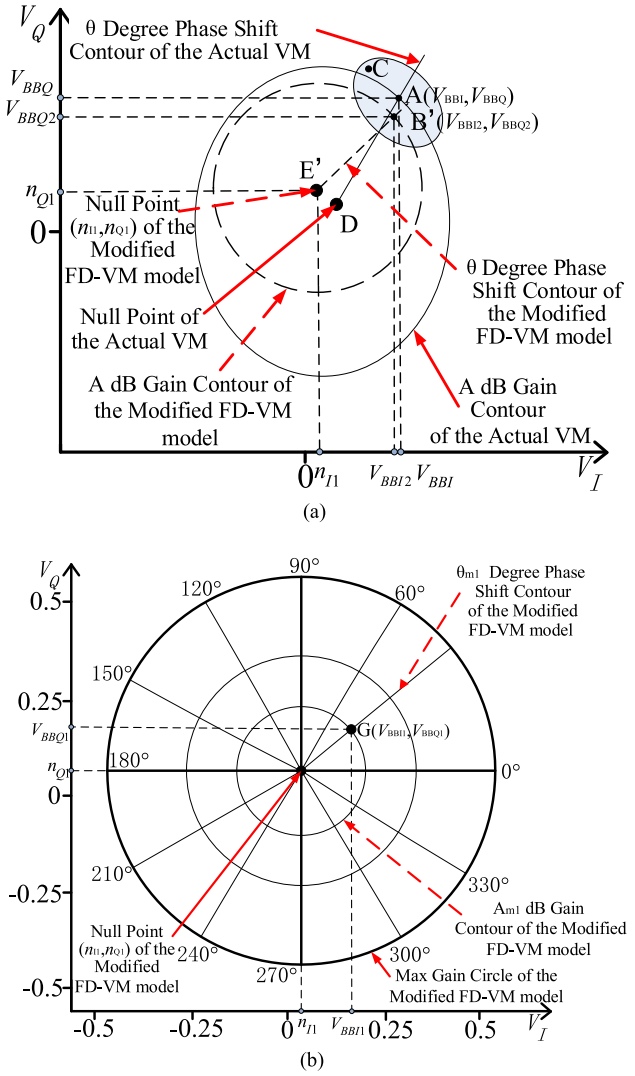

FIGURE 6. Sketch illustrating (a) the transmission amplitude, A, and phase shift, θ, contours of the actual VM and the modified FD-VM model at frequency f. (b) The transmission amplitude and phase contour plots of the modified FD-VM model at frequency f.

corresponding transmission state (A and θ). It indicates that if two of the three parameters are given, the other parameter is computable by solving equation (3). Now, since (V_{BBI1}, V_{BBQ1}) and (A_{m1} and θ_{m1}) are given, the shift vector pair could be calculated as n_{I1} and n_{Q1}. As the obtained shift vector pair in this step may not be accurate enough to formulate the transfer function with the required accuracy, it is written as (n_{I1}, n_{Q1}) but not (n_I, n_Q), which is regarded as the theoretically best suited shift vector pair for a certain transmission state. By introducing n_I and n_Q, equation (3) is able to be modified through measurements. Note that (n_I, n_Q) is only valid within certain transmission amplitude and phase control ranges, because it is calculated from certain baseband control voltages and the corresponding measured transmission state. Therefore, (n_I, n_Q) varies with the desired transmission state.

Now, since (n_{I1}, n_{Q1}) is obtained for equation (3), it is capable of predicting a more accurate baseband control voltage pair (V_{BBI2}, V_{BBQ2}) for the desired transmission state. After (V_{BBI2}, V_{BBQ2}) is achieved, the corresponding measured transmission amplitude and phase of the actual VM are regarded as A_{m2} and θ_{m2}, respectively. Through a set of measurements, it is found that A_{m2} and θ_{m2} is usually acceptable for general applications, in which the amplitude and phase control accuracy are about 1 dB and 5°, respectively. If more accurate control of the transmission state is needed, further iteration procedures are required. The procedure of the transfer function extraction mentioned above is illustrated by the flowchart in Fig. 7.

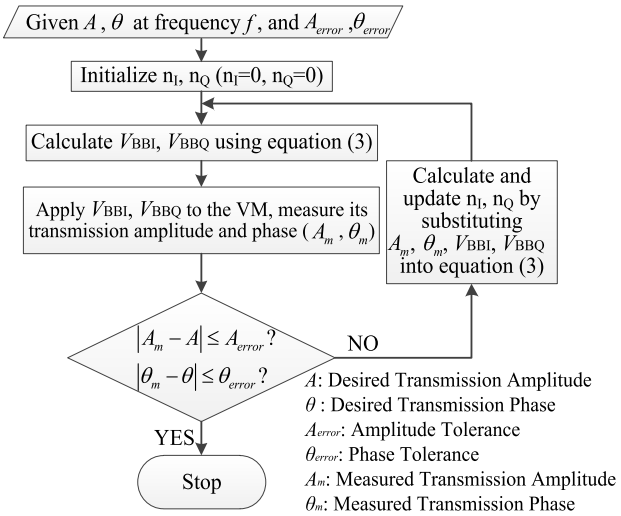

FIGURE 7. The flowchart of the proposed transfer function extraction process.

The extracted transfer function is also valid within certain amplitude and phase control ranges. As illustrated in Fig. 6(a), assuming that point A corresponds to a transmission state point, and the transfer function is already extracted at this point. Then, the relationship between the control voltages and the transmission states near to point A, is able to be approximately described by the extracted transfer function at point A. In Fig. 6(a), the shaded region is used to illustrate the transmission states near to point A. Taking point C, which is located in the shaded region near to point A, as an example, since point C is in the vicinity of point A, the transfer functions associated with the two points are close to each other. Therefore, it is feasible to apply the transfer function extracted at point A to point C, though the accuracy may decrease.

D. A PRACTICAL STEP-BY-STEP PROCEDURE FOR THE TRANSFER FUNCTION EXTRACTION

Step 1) Set up the reference transmission state of the VM. Theoretically, the reference transmission state is supposed to be arbitrary as long as it is achievable for the VM. In practice, by selecting appropriate baseband control voltages and

then applying them to the VM, the corresponding reference transmission state is obtained.

Step 2) Determine the systematic insertion phase ($Phase_{\text{const}}(f)$) of the VM. By assuming that the insertion phase of the VM core circuit is zero, when it is in the reference transmission state, $Phase_{\text{const}}(f)$ is able to be achieved by measuring the reference transmission state of the VM. After obtaining the S21 of the VM through measurements, $Phase_{\text{const}}(f)$ is determined as:

$$Phase_{const}\,(f) = \angle S21 \tag{4}$$

Step 3) Determine the insertion loss of the total frequency-dependent part ($Gain_{\text{const}}(f)$) of the VM. $Gain_{\text{const}}(f)$ can be obtained as the insertion loss of the VM when it is in the reference transmission state. Adopting the measured S parameter in Step 2), $Gain_{\text{const}}(f)$ is able to be formulated as:

$$Gain_{const}\,(f) = |S21| \tag{5}$$

Step 4) As $Phase_{\text{const}}(f)$ and $Gain_{\text{const}}(f)$ are extracted, for the following transfer function extraction procedure, please refer to the flowchart in Fig. 7.

III. EXPERIMENTAL VERIFICATION

To validate the transfer function extraction approach, it is applied to a VM module, which is shown in Fig. 3(a). The Cartesian VM chip AD8341 and the associated distributed components are adopted to compose the core circuit of the VM, which is depicted in Fig. 3(b). A detailed description of the VM under test and the corresponding measurement setup are presented in our previous work [20].

The requirements for the VM manipulation are that the desired complex gain is -4.5 dB$\angle 30°$ at 1700 MHz and that the corresponding phase and amplitude tolerances are $\pm 0.3°$ and ± 0.05 dB, respectively. It is notable that the proposed -4.5 dB$\angle 30°$ complex gain is just an example for the experimental verification, and the complex gain is able to be any arbitrary complex value as long as it is within the phase and amplitude control ranges of the VM hardware.

According to the procedure of the transfer function extraction explained in Section II. D, the systematic insertion phase of the VM and the insertion loss of the total frequency-dependent part of the VM are obtained, which are depicted as the green line and blue dotted line, respectively, in Fig. 8. It shows that both the insertion loss and the systematic insertion phase are frequency-dependent.

From Fig. 8, $Phase_{\text{const}}(f)$ and $Gain_{\text{const}}(f)$ are $-67.62°$ and -3.77 dB, respectively, at the frequency point of 1700 MHz. Then, by implementing the procedure of the transfer function extraction, the baseband control voltages, the extracted shift vector and the corresponding measured transmission state data are obtained, which are shown in Table 1.

After the 1st iteration, the measured complex gain is -4.69 dB$\angle 31.28°$, which is outside the tolerance of the desired transmission state. Therefore, a second iteration procedure is implemented, in order to obtain a more appropriate shift vector pair for the transfer function. After the 2nd iteration, the extracted transfer function is sufficient to predict the required baseband control voltages for the desired transmission state, since the measured complex gain is -4.47 dB$\angle 30.12°$, which is within the tolerance requirement.

To further illustrate the validity and the performance of the proposed calibration method, certain phase and amplitude control ranges are calibrated by this method, which cover the full 360° phase shift range with a 1° phase shift step, over the -16.5 to -4.5 dB gain control range with a gain step of 3 dB. Fig. 9 illustrates the uncalibrated and calibrated amplitude

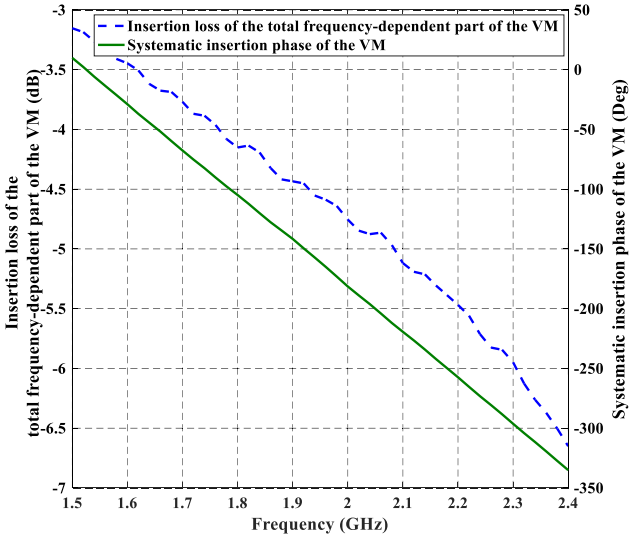

FIGURE 8. The systematic insertion phase of the VM and the insertion loss of the total frequency-dependent part of the VM.

TABLE 1. Extracted parameters and the associated measurement results.

The desired gain/phase is -4.5 dB/30° at f=1700 MHz, and the gain/phase tolerance is ±0.05 dB/±0.3°			
Name	**Iteration 0**	**Iteration 1**	**Iteration 2**
n_{I}	0 V	0.026841 V	0.035465 V
n_{Q}	0 V	0.026014 V	0.037315 V
V_{I}	-0.060956 V	-0.034115 V	-0.025491 V
V_{Q}	0.455635 V	0.481649 V	0.492951 V
Measured *Gain*	-4.91 dB	-4.69 dB	-4.47 dB
Measured *Phase*	33.93°	31.28°	30.12°
Gain error	-0.41 dB	-0.19 dB	0.03 dB
Phase error	3.93°	1.28°	0.12°

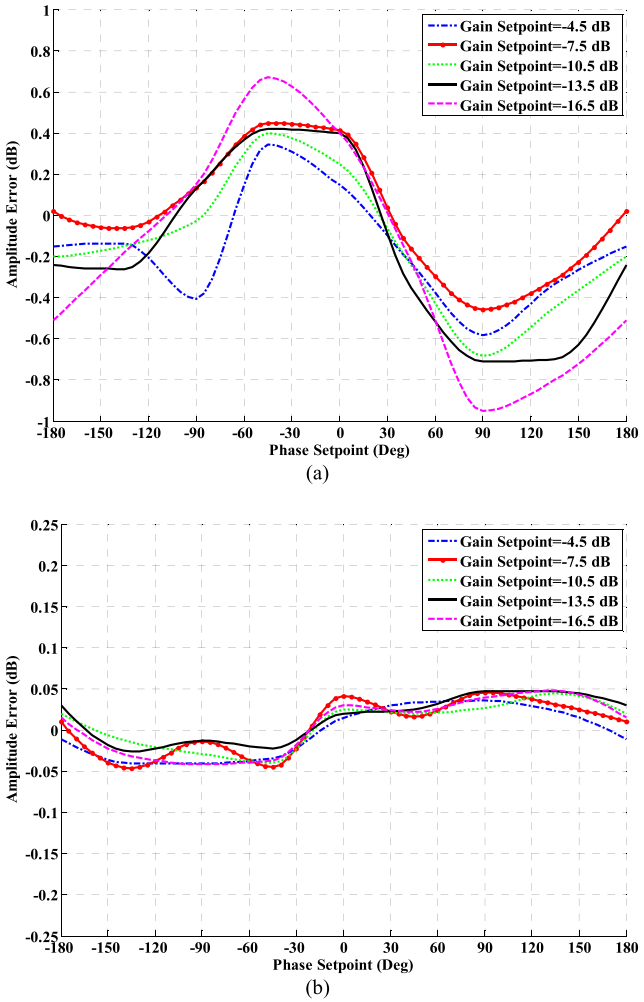

FIGURE 9. Amplitude error versus the phase setpoint at different gain setpoints (frequency of 1700 MHz): (a) uncalibrated case; (b) calibrated case.

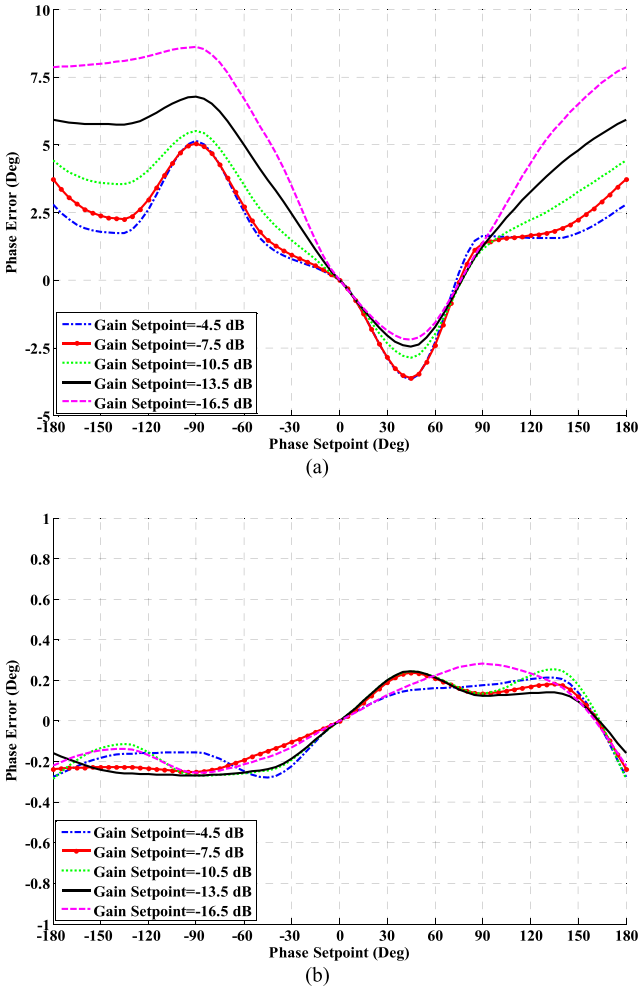

FIGURE 10. Phase error versus the phase setpoint at different gain setpoints (frequency of 1700 MHz): (a) uncalibrated case; (b) calibrated case.

error versus the desired phase setpoints for different gain setpoints at 1700 MHz. The maximum error of the uncalibrated amplitude over the −16.5 to −4.5 dB gain control range reaches 0.95 dB, but it is reduced to 0.05 dB after calibration. Fig. 10 shows the uncalibrated and calibrated phase error against the desired phase setpoints at different gain setpoints. The maximum error of the uncalibrated phase over the whole gain control range is 8.7°, while it is below 0.3° after the calibration. It should be mentioned that the calibration results in Fig.9 (b) and Fig.10 (b) are achieved after only two iterations. Fig. 11 and Fig. 12 present the absolute value of the amplitude and phase errors versus the iteration number at different complex gain setpoints, respectively. It shows that the iteration loop converges within only a few iteration steps. The maximum amplitude and phase errors at different complex gain setpoints are reduced to 0.05 dB and 0.3°, respectively, after two iteration steps. The experimental results verify that the proposed calibration method is capable of accurately describing the relationship between the complex gain and the corresponding baseband control voltages of the actual VM, after only a few iterations. Meanwhile, the iteration loop converges very quickly after only two steps. Due to the high accuracy and fast convergence, the proposed method is suitable for high-accuracy and real-time calibration applications.

As previously mentioned in the last paragraph of Section II. C, the extracted transfer function is also capable of predicting the baseband control voltages for other desired transmission states, which are close to the transfer function extracted transmission state. Taking the transmission state of −4.5 dB∠30° for example, the transfer function is extracted at this transmission state, and the parameters of the extracted transfer function are listed in Table 1. Therefore, other desired transmission states near to −4.5 dB∠30° can also be described by the extracted transfer function of the −4.5 dB∠30° transmission state, and the corresponding measurement results are listed in Table 2. In this table, the transmission state of −4.5 dB∠30° corresponds to point A in Fig. 6(a), and the remained transmission states are assumed to be located in the shaded region in Fig. 6(a).

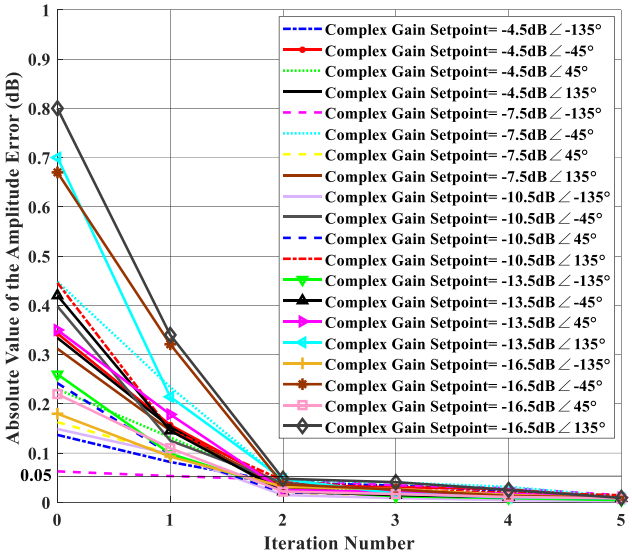

FIGURE 11. Absolute value of the amplitude error versus the iteration number at different complex gain setpoints (frequency of 1700 MHz).

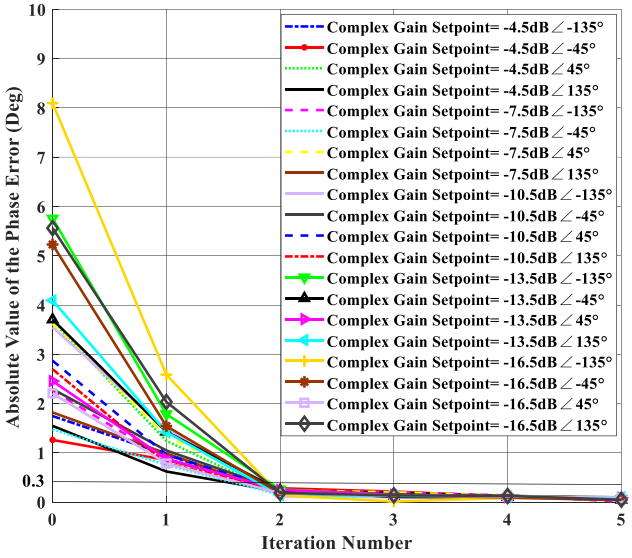

FIGURE 12. Absolute value of the phase error versus iteration number at different complex gain setpoints (frequency of 1700 MHz).

TABLE 2. The measurement results for other desired transmission states near to the extracted transmission state (−4.5 dB∠30°).

Desired		Measured		Error	
G (dB)	P (°)	G (dB)	P (°)	G (dB)	P (°)
-4.5	20	-4.36	19.06	0.14	-0.94
	25	-4.43	24.56	0.07	-0.44
	26	-4.44	25.74	0.06	-0.26
	27	-4.45	26.82	0.05	-0.18
	28	-4.45	27.89	0.05	-0.11
	29	-4.43	28.98	0.07	-0.02
	30	-4.47	30.12	0.03	0.12
	31	-4.42	31.34	0.08	0.34
	32	-4.43	32.38	0.07	0.38
	33	-4.47	33.42	0.03	0.42
	34	-4.46	34.67	0.04	0.67
	35	-4.45	35.87	0.05	0.87
	40	-4.44	41.56	0.06	1.56
-7.5	20	-7.41	18.49	0.09	-1.51
	25	-7.45	24.12	0.05	-0.88
	30	-7.45	29.61	0.05	-0.39
	31	-7.48	30.53	0.02	-0.47
	32	-7.47	31.55	0.03	-0.45
	33	-7.48	32.68	0.02	-0.32
	34	-7.48	33.75	0.02	-0.25
	35	-7.49	34.92	0.01	-0.08
	40	-7.48	40.48	0.02	0.48
-10.5	25	-10.51	24.06	-0.01	-0.94
	30	-10.51	29.54	-0.01	-0.46
	35	-10.51	35.18	-0.01	0.18
-13.5	25	-13.74	23.42	-0.24	-1.58
	30	-13.71	29.02	-0.21	-0.98
	35	-13.68	34.23	-0.18	-0.77
-16.5	25	-16.93	23.13	-0.43	-1.87
	30	-16.93	28.84	-0.43	-1.16
	35	-16.95	34.11	-0.45	-0.89

By investigating the measurement results in Table 2, it shows that within an amplitude control range of 6 dB (−10.5 to −4.5 dB) and a corresponding phase control range of 10° (25° to 35°), the phase and amplitude errors between the measured transmission states and the desired are within ±1° and ±0.1 dB, respectively. Therefore, the extracted transfer function is valid within certain amplitude and phase control ranges.

IV. DISCUSSION

From the procedure of the transfer function extraction, it shows that the proposed method is directly aimed at calculating the required control voltages for the desired transmission state through a transfer function model. This approach is more efficient than the sweep control signal method, in which a great deal of data points should be tested. For example, in a specific application, the control requirements for the transmission phase and amplitude are: (1) the transmission phase and amplitude tolerance are ±1° and ±0.1 dB, respectively; (2) 360° phase shift control range with a 5° control step; (3) amplitude control range of 6 dB with a 0.75 dB control step. Based on the proposed approach, only approximately 36 pairs of the shift vector are needed to be extracted. Since each shift vector pair is able to cover 6 dB of amplitude control range and 10° of phase control range, which is observed in Section III and validated by additional measurements. The benefit of the proposed method is evident, since two iteration steps are normally sufficient to extract the shift vector, and the procedure for extracting 36 pairs

of the shift vector only requires approximately 108 times of evaluation for the transmission state of the actual VM. Meanwhile, only 36 pairs of the shift vector data are needed to be stored. In comparison, 576 pairs of the baseband control voltage should be stored for the sweep control signal method. Furthermore, a tremendous number of points, which are far greater than 576 are required to be swept on the constellation and measured to extract the desired transmission state. In [28], 15991 data points were required to be tested, in order to obtain a 360° phase shift control range with a 5.625° control step and a corresponding amplitude control range of 6 dB with a 0.75 dB control step. Compared to the model-based calibration method in [29] and [30], the calibration method proposed here is relatively highly efficient, since the model parameters are able to be extracted in a few iterations, while the model parameters extraction process by parameter sweeping in [29] and [30] is relatively inefficient. Meanwhile, the frequency-dependent insertion phase and loss of the actual VM are also included in this approach, which cannot be seen in [17]. For the calibration accuracy, the performance of the proposed calibration method and other reported works are listed in Table 3. As can be observed, the proposed method shows relatively higher calibration accuracy. In recent years, the state-of-the-art VM MMICs have adopted an on-chip calibration unit, which adopts a extractor circuit for transmission amplitude and phase errors, and a dedicated calibration scheme [7], [9], [31]. The desired transmission state can be quickly obtained with high accuracy, by using the proposed VM MMICs and the corresponding calibration scheme. However, these calibration schemes are only applicable to dedicated VM MMICs.

TABLE 3. Comparison of calibration accuracy between the proposed method and conventional methods.

Ref.	Frequency	Calibrated Amplitude Error	Calibrated Phase Error
This work	1.7GHz	0.05dB	0.3°
[17]	200.222MHz	0.05dB	0.5°
[25]	1.6GHz	0.21dB	1.3°
[30]	1.575GHz	0.2dB	0.5°

The proposed calibration approach is mainly focused on effectively obtaining the correct control voltages for the desired transmission states. This is because, in most cases, the end users of the VM are only interested in how to obtain the required control voltages for the desired transmission amplitude and phase with high efficiency and accuracy. Indeed, the imperfections inside the VM chip and the nonideal behavior of the peripheral circuit of the VM chip will influence the final performance of the VM assembly, but these aspects are usually beyond the control of the end users. Therefore, calibrating for the control voltages is an appropriate method to achieve the desired transmission state of the VM. In order to obtain the calibrated control voltages for an actual VM, the contours of the transmission amplitude and phase of the modified FD-VM model are shifted in the control voltage plane, until the predicted transmission state of the model matches the desired transmission state. For the VM models, which describe all of the practical nonideal aspects of the actual VM, could be developed to calibrate the actual VM. However, in order to obtain the model parameters, a large number of measurements are required. In comparison, the modified FD-VM model developed here is a behavioral model of the actual VM, which is not restricted to the specific nonideal characteristics of the actual VM, such as the phase and amplitude imbalances, the imperfect input 90° hybrid and the output combiner. After only several iterations, the calibrated control voltages for the desired transmission state are able to be obtained by this approach. For the evaluation of the transmission amplitude and phase in system-level applications, the amplitude and phase error detection scheme developed in [32] could be adopted. From the discussions, it can be concluded that the proposed calibration method is well suited for real-time calibration scenarios and multichannel VM system calibration.

V. CONCLUSION

In this paper, a calibration method based on transfer function extraction for the Cartesian VM is presented. Three kinds of VM models and their transfer functions are developed. At the desired transmission state point, the transfer function of the modified FD-VM model are able to be extracted from the measured transmission state data of the actual VM by iteration. Then, the extracted transfer function is able to calibrate the actual VM. The experimental results show that, the transfer function is extracted after only two iteration steps, and the calibrated amplitude and phase errors of the actual VM are less than 0.05 dB and 0.3°, respectively, these validate the high accuracy and high efficiency of the proposed calibration method. Meanwhile, the extracted transfer function is also valid within certain transmission amplitude and phase control ranges; thus, less memory is required to store the model parameters. Moreover, this method is not limited to the specific nonideal behavior of the actual VM. With the advantages presented above, this technique is suitable for a variety of applications, especially in multichannel VM system calibration and real-time calibration scenarios.

REFERENCES

[1] A. Hajimiri, A. Komijani, A. Natarajan, R. Chunara, X. Guan, and H. Hashemi, "Phased array systems in silicon," *IEEE Commun. Mag.*, vol. 42, no. 8, pp. 122–130, Aug. 2004.
[2] J. Paramesh, R. Bishop, K. Soumyanath, and D. J. Allstot, "A four-antenna receiver in 90-nm CMOS for beamforming and spatial diversity," *IEEE J. Solid-State Circuits*, vol. 40, no. 12, pp. 2515–2524, Dec. 2005.
[3] J. G. Colom, L. G. Castaneda, and E. Knapp, "Phase shifter system using vector modulation for xband phased array radar applications," in *Proc. IEEE Int. Geosci. Remote Sens. Symp. (IGARSS)*, Barcelona, Spain, Jul. 2007, pp. 2750–2753.
[4] R. Eickhoff, R. Kraemer, I. Santamaria, and L. Gonzalez, "Developing energy-efficient MIMO radios," *IEEE Veh. Technol. Mag.*, vol. 4, no. 1, pp. 34–41, Mar. 2009.

[5] S. Kumar, "Directly modulated VSAT transmitter," *Microw. J.*, vol. 33, no. 4, pp. 255–264, Apr. 1990.
[6] U. Mayer, M. Wickert, R. Eickhoff, and F. Ellinger, "Multiband mixed-signal vector modulator IC," in *Proc. IEEE Radio Freq. Integr. Circuits Symp.*, Baltimore, MD, USA, Jun. 2011, pp. 1–4.
[7] R. Singh, S. Mondal, and J. Paramesh, "A 25.1-27.6 GHz tunable-narrowband digitally-calibrated merged LNA-vector modulator for 5G phased arrays," in *Proc. IEEE Radio Freq. Integr. Circuits Symp. (RFIC)*, Philadelphia, PA, USA, Jun. 2018, pp. 4–7.
[8] I. Kalyoncu, A. Burak, M. Kaynak, and Y. Gurbuz, "A 26-GHz vector modulator in 130-nm SiGe BiCMOS achieving monotonic 10-b phase resolution without calibration," in *Proc. IEEE Radio Freq. Integr. Circuits Symp. (RFIC)*, Boston, MA, USA, Jun. 2019, pp. 75–78.
[9] R. Singh, S. Mondal, and J. Paramesh, "A compact digitally-assisted merged LNA vector modulator using coupled resonators for integrated beamforming transceivers," *IEEE Trans. Microw. Theory Techn.*, vol. 67, no. 7, pp. 2555–2568, Jul. 2019.
[10] S. Shahramian, M. J. Holyoak, A. Singh, and Y. Baeyens, "A fully integrated 384-element, 16-tile, W-Band phased array with self-alignment and self-test," *IEEE J. Solid-State Circuits*, vol. 54, no. 9, pp. 2419–2434, Sep. 2019.
[11] E. E. Eid and F. M. Ghannouchi, "Adaptive nulling loop control for 1.7-GHz feedforward linearization systems," *IEEE Trans. Microw. Theory Techn.*, vol. 45, no. 1, pp. 83–86, Jan. 1997.
[12] K. Lin, Y. E. Wang, C.-K. Pao, and Y.-C. Shih, "A Ka-band FMCW radar front-end with adaptive leakage cancellation," *IEEE Trans. Microw. Theory Techn.*, vol. 54, no. 12, pp. 4041–4048, Dec. 2006.
[13] L. Silverman and C. D. Plato, "Vector modulator enhances feed-forward cancellation," *Microw. RF*, vol. 37, no. 3, pp. 83–90, Mar. 1998.
[14] R. Tseng, H. Li, D. H. Kwon, Y. Chiu, and A. S. Y. Poon, "A four-channel beamforming down-converter in 90-nm CMOS utilizing phase-oversampling," *IEEE J. Solid-State Circuits*, vol. 45, no. 11, pp. 2262–2272, Nov. 2010.
[15] M. C. M. Soer, E. A. M. Klumperink, D.-J. van den Broek, B. Nauta, and F. E. van Vliet, "Beamformer with constant-gm vector modulators and its spatial intermodulation distortion," *IEEE J. Solid-State Circuits*, vol. 52, no. 3, pp. 735–746, Mar. 2017.
[16] U. Mayer, M. Wickert, R. Eickhoff, and F. Ellinger, "2–6-GHz BiCMOS polar-based vector modulator for S- and C-band diversity receivers," *IEEE Trans. Microw. Theory Techn.*, vol. 60, no. 3, pp. 567–573, Mar. 2012.
[17] P. Tošovský and D. Valúch, "Improvement of RF vector modulator performance by feed-forward based calibration," *Radioengineering*, vol. 19, no. 4, pp. 627–632, Dec. 2010.
[18] O. Manu, M. Dimian, and A. Graur, "Influence of quantization errors on the development of vector modulator based phaseshifter for use in smart antenna applications," in *Proc. IEEE 17th Int. Symp. Design Technol. Electron. Packag. (SIITME)*, Timişoara, Romania, Oct. 2011, pp. 283–286.
[19] I. Rutkowski, K. Czuba, D. Makowski, A. Mielczarek, H. Schlarb, and F. Ludwig, "Vector modulator card for MTCA-based LLRF control system for linear accelerators," *IEEE Trans. Nucl. Sci.*, vol. 60, no. 5, pp. 3609–3614, Oct. 2013.
[20] C. Wang and J. Miao, "Implementation and broadband calibration of a multichannel vector modulator module," *IET Sci., Meas. Technol.*, vol. 11, no. 2, pp. 155–163, Mar. 2017.
[21] F. Hutu, D. Cordeau, and J. M. Paillot, "2.4 GHz antenna array using vector modulator based active phase shifters for beamforming," *IET Microw., Antennas Propag.*, vol. 5, no. 2, pp. 245–254, Jan. 2011.
[22] B.-H. Ku and S. Hong, "6-bit CMOS digital attenuators with low phase variations for X-band phased-array systems," *IEEE Trans. Microw. Theory Techn.*, vol. 58, no. 7, pp. 1651–1663, Jul. 2010.
[23] H. Wang and A. Hajimiri, "A Wideband CMOS linear digital phase rotator," in *Proc. CICC*, San Jose, CA, USA, 2007, pp. 671–674.
[24] A. E. Ashtiani, S.-I. Nam, A. d'Espona, S. Lucyszyn, and I. D. Robertson, "Direct multilevel carrier modulation using millimeter-wave balanced vector modulators," *IEEE Trans. Microw. Theory Techn.*, vol. 46, no. 12, pp. 2611–2619, Dec. 1998.
[25] J. Grajal, J. Gismero, M. Mahfoudi, and F. A. Petz, "A 1.4-2.7-GHz analog MMIC vector modulator for a crossbar beamforming network," *IEEE Trans. Microw. Theory Techn.*, vol. 45, no. 10, pp. 1705–1714, Oct. 1997.
[26] D. S. McPherson and S. Lucyszyn, "Vector modulator for W-band software radar techniques," *IEEE Trans. Microw. Theory Techn.*, vol. 49, no. 8, pp. 1451–1461, Aug. 2001.
[27] M. Kantanen, J. Holmberg, M. Varonen, and A. Rantala, "Digitally controlled vector modulator SiGe MMIC for millimeter-wave phased array applications," in *Proc. 11th German Microw. Conf. (GeMiC)*, Freiburg im Breisgau, Germany, Mar. 2018, pp. 51–54.
[28] Y. Shang, H. Luo, F. Yu, L. Wang, B. Li, and H. Zhang, "An efficient testing system and calibration method for a reflection type vector modulator," *Measurement*, vol. 46, no. 10, pp. 3802–3807, Dec. 2013.
[29] E. Juntunen, J. Laskar, J. Papapolymerou, and D. Dawn, "CMOS 45 GHz vector modulator with gain/phase correction through calibration," *Electron. Lett.*, vol. 49, no. 4, pp. 267–269, Feb. 2013.
[30] J. M. Blas and J. I. Alonso, "Low cost wideband I-Q vector modulator," *Electron. Lett.*, vol. 33, no. 1, pp. 18–20, Jan. 1997.
[31] W.-J. Jung, N.-P. Hong, K.-H. Nam, J.-H. Lee, T.-J. Kim, P. Jang, and J.-S. Park, "An improved vector modulator using Q-factor calibration for 5–6 GHz beamforming receiver," in *Proc. Int. Conf. Electron., Inf., Commun. (ICEIC)*, Honolulu, HI, USA, Jan. 2018, pp. 1–5.
[32] S.-M. Moon, H. L. Lee, I.-B. Yom, and M.-Q. Lee, "Reconfigurable K-band MIMO transmission with on-board vector calibration," *IEEE Access*, vol. 6, pp. 49358–49365, 2018.

CHAO WANG received the M.S.E.E. and Ph.D. degrees from the School of Electronics and Information Engineering, Beihang University, Beijing, China, in 2014 and 2019, respectively. He is currently a Lecturer with Zhengzhou University, Zhengzhou, China. His current research interests include RF circuit design and microwave imaging techniques, wireless sensing, and 5G.

XIANG-RUI CHENG is currently pursuing the bachelor's degree with Zhengzhou University, Zhengzhou, China. His current research interests include RF systems, wireless sensing, the IoT, and 5G.

YIN-XIN SUN is currently pursuing the bachelor's degree with Zhengzhou University, Zhengzhou, China. His current research interests include RF systems, wireless sensing, the IoT, and 5G.

PENG-SONG DUAN received the M.Sc. degree in computer science from Chongqing University, Chongqing, China, in 2007. He is currently pursuing the Ph.D. degree in software engineering with Zhengzhou University, Zhengzhou, China. He is currently a Lecturer with Zhengzhou University. His current research interests include wireless sensing, the IoT, and machine learning.

YANG-JIE CAO received the M.Sc. degree in computer science from Zhengzhou University, Zhengzhou, China, in 2006, and the Ph.D. degree in computer science from Xi'an Jiaotong University, Xi'an, China, in 2012. He is currently an Associate Professor with Zhengzhou University. His current research interests include wireless sensing, intelligent computing, artificial intelligence, and high-performance computing.